A highly selective humanized DDR1 mAb reverses immune exclusion by disrupting collagen fiber alignment in breast cancer

Junquan Liu,[1] Huai-Chin Chiang,[2] Wei Xiong,[1] Victor Laurent,[3] Samuel C Griffiths ![ORCID],[4] Jasmin Dülfer ![ORCID],[5] Hui Deng,[1] Xiujie Sun,[2] Y Whitney Yin,[6] Wenliang Li,[1] Laurent P Audoly,[7] Zhiqiang An ![ORCID],[1] Thomas Schürpf ![ORCID],[7] Rong Li,[2] Ningyan Zhang[1]

ABSTRACT

Background Immune exclusion (IE) where tumors deter the infiltration of immune cells into the tumor microenvironment has emerged as a key mechanism underlying immunotherapy resistance. We recently reported a novel role of discoidin domain-containing receptor 1 (DDR1) in promoting IE in breast cancer and validated its critical role in IE using neutralizing rabbit monoclonal antibodies (mAbs) in multiple mouse tumor models.

Methods To develop a DDR1-targeting mAb as a potential cancer therapeutic, we humanized mAb9 with a complementarity-determining region grafting strategy. The humanized antibody named PRTH-101 is currently being tested in a Phase 1 clinical trial. We determined the binding epitope of PRTH-101 from the crystal structure of the complex between DDR1 extracellular domain (ECD) and the PRTH-101 Fab fragment with 3.15 Å resolution. We revealed the underlying mechanisms of action of PRTH-101 using both cell culture assays and *in vivo* study in a mouse tumor model.

Results PRTH-101 has subnanomolar affinity to DDR1 and potent antitumor efficacy similar to the parental rabbit mAb after humanization. Structural information illustrated that PRTH-101 interacts with the discoidin (DS)-like domain, but not the collagen-binding DS domain of DDR1. Mechanistically, we showed that PRTH-101 inhibited DDR1 phosphorylation, decreased collagen-mediated cell attachment, and significantly blocked DDR1 shedding from the cell surface. Treatment of tumor-bearing mice with PRTH-101 *in vivo* disrupted collagen fiber alignment (a physical barrier) in the tumor extracellular matrix (ECM) and enhanced CD8+ T cell infiltration in tumors.

Conclusions This study not only paves a pathway for the development of PRTH-101 as a cancer therapeutic, but also sheds light on a new therapeutic strategy to modulate collagen alignment in the tumor ECM for enhancing antitumor immunity.

WHAT IS ALREADY KNOWN ON THIS TOPIC

⇒ Discoidin domain-containing receptor 1 (DDR1) plays an important role in cancer progression. However, the DDR1 function in tumors is still elusive. We recently reported that DDR1 promoted collagen fiber alignment and formation of a physical barrier, which causes immune exclusion from tumors.[17] We also demonstrated that our DDR1 ECD-targeting mAbs can disrupt collagen fiber alignment and increase T cell infiltration in tumors.

WHAT THIS STUDY ADDS

⇒ In this study, we humanized a DDR1 ECD-targeting mAb and showed significant antitumor efficacy in an immunocompetent mouse model. We determined the binding epitope using gene mutagenesis, hydrogen-deuterium exchange mass spectrometry, and X-ray crystallography. Mechanistically, we showed that the humanized mAb inhibited DDR1 phosphorylation and, more importantly, blocked DDR1 shedding and disrupted a physical barrier formed by collagen fiber alignment in tumors.

HOW THIS STUDY MIGHT AFFECT RESEARCH, PRACTICE OR POLICY

⇒ This study not only paves a pathway for development of PRTH-101 as a cancer therapeutic, but also broadens our understanding of the roles of DDR1 in modulation of collagen alignment in tumor extracellular matrix and tumor immune microenvironment.

BACKGROUND

Immune cells in the tumor microenvironment (TME) play an important role in cancer development and progression.[1 2] Increased tumoral infiltration of cytotoxic CD8+ T cells has been associated with improved clinical outcomes.[3 4] Immune exclusion (IE) in solid tumors is characterized by a low density of T cell infiltration in the tumor epithelium and T cell enrichment in the tumor stroma.[5] IE tumors or immune-deserted cold tumors with low or no immune cell infiltrations are often associated with poor outcomes and poor respond to current cancer immunotherapies.[6]

Therefore, therapeutic strategies for modulation of the TME and enhancing cytotoxic T cell infiltration in IE solid tumors are critically needed.

Discoidin domain-containing receptor 1 (DDR1) is a receptor tyrosine kinase and has many important physiological functions in cells.[7] Dysregulation of DDR1 has been implicated in various human diseases including cancers.[8 9] A study reported that DDR1 promoted cancer progression by regulating the interaction between tumor cells and collagen matrix[10] and overexpression of DDR1 promoted tumor growth *in vivo*.[11] Several studies reported that increased expression of DDR1 correlated with tumor progression in various types of cancer.[12–16] We recently revealed a negative correlation between DDR1 expression and CD8^{+} T cells in tumors and demonstrated that DDR1 interaction with collagen played an important role in T cell exclusion in the TME.[17] DDR1 is activated by binding of either fibrillar collagens (types I–III and V) or non-fibrillar collagens (type IV collagen) to its discoidin (DS) domain.[18] On collagen binding, DDR1 clusters on the cell surface and undergoes tyrosine autophosphorylation, triggering a series of downstream signaling pathways.[19] Simultaneously, collagen binding induces shedding of DDR1 by a membrane-bound metalloproteinase.[20] The shed DDR1 ECD, but not its intracellular kinase domain, is required for IE in breast cancer.[17]

In this study, we characterized an efficacious humanized monoclonal antibody targeting DDR1 as a preclinical candidate (PRTH-101) for development as a potential anticancer therapeutic. We determined the binding epitope of PRTH-101 on the DS-like (DSL) domain of DDR1, which is distal to the collagen-binding site on the DS domain of DDR1. Mechanistically, we revealed that PRTH-101 blocked DDR1 ECD shedding and employed multiple mechanisms of action in targeting the DDR1/collagen axis. Significantly, treatment of tumor-bearing mice with PRTH-101 reversed IE by disrupting collagen fiber alignment surrounding the tumors and enhanced T cells infiltration into the TME.

METHODS
Cell lines
HEK293F, HEK293T and T47D were obtained from ATCC. The murine breast cancer cell line E0771 was obtained from CH3 BioSystems. Engineered cell lines *Ddr1*-KO E0771 (E0771-KO), *Ddr1*-KO, empty vector-reconstituted E0771 (E0771-EV) and *Ddr1*-KO, *hDDR1*-reconstituted E0771 (E0771-hDDR1) are described in our previous study.[17] The DDR1 overexpressing HEK293 (HEK293-DDR1) cell line was constructed by transducing HEK293T cells with a lenti-vector containing a human DDR1 (full length) gene construct. T47D was cultured in Roswell Park Memorial Institute (RPMI) 1640 media (catalog no. 10-040-CV, Corning) with 10% fetal bovine serum (FBS, catalog no. F0900-050, GenDEPOT). HEK293T and E0771 and its derivatives were cultured in Dulbecco's Modified Eagle Medium (DMEM, catalog no. 10-013-CV, Corning) with 10% FBS.

Migration assay with transwell
Immune cell migration assay with transwell (catalog no. 3421, Corning) was performed using mouse splenocytes isolated from C57BL/6 mice. Briefly, E0771-KO and E0771-hDDR1 cancer cells were cultured for 48 hours. The cancer cell conditioned culture media were collected by centrifugation to pellet cells, and pre-incubated with antibody for 1 hour to neutralize DDR1 in the conditioned media. The conditioned media with DDR1 and antibody were then transferred to the bottom chamber of the transwell, and splenocytes were placed in the upper chamber. After 2 hours, migratory splenocytes were collected from the lower membrane chamber and quantified by flow cytometry analysis.

Affinity measurement with biolayer interferometry assay
The affinity of mAbs for hDDR1 ECD or mouse DDR1 (mDDR1) ECD was measured on an Octet RED96 system (ForteBio). Briefly, 30 µg/mL of mAb was captured by protein A biosensors (ForteBio) for 5 min. Following a brief equilibration in kinetics buffer (ForteBio), the loaded biosensors were exposed to a series of three-fold diluted hDDR1 ECD or mDDR1 ECD. The association step lasted for 5 min and was followed by a dissociation step with kinetics buffer for 10 min. A reference biosensor loaded only with antibody was used for background correction. The association and dissociation rates were obtained by fitting the data to a 1:1 binding model. The K_D value was calculated using k_{off}/k_{on}.

ELISA binding assay
High binding Corning 96-well plates (catalog no. 9018, Corning) were coated with 1 µg/mL of hDDR1 ECD (100 µL) overnight at 4°C, followed by blocking for 2 hours with 5% non-fat milk. After washing with PBST (0.05% Tween-20) three times, 100 µL of threefold serially diluted rabbit or humanized antibodies were added and incubated for 1 hour at room temperature (RT). Following three times of wash with PBST, the secondary anti-rabbit F(ab')$_2$ or anti-human F(ab')$_2$ HRP-conjugated IgG (catalog no. 111-036-047 and 109-035-006, Jackson ImmunoResearch) were added and incubated for 1 hour at RT. After washing with PBST three times, 100 µL of TMB substrate was added and incubated for about 10 min at RT. The reaction was stopped by addition of 50 µL of 1 M sulfuric acid and absorbance at 450 nm was measured using a spectrophotometer (Molecular Devices).

Humanization of rabbit anti-DDR1 mAb
Rabbit anti-DDR1 mAb humanization was performed via grafting combined Kabat/IMGT/Paratome complementarity-determining regions (CDR) as described previously.[21] Briefly, CDRs in the rabbit mAb heavy chain and light chain were defined by a combined Kabat/IMGT/Paratome method. After aligning the rabbit mAb with the closest human germline sequence,

residues that are not structurally critical were identified and humanized. The humanized variable fragments (VH and VL) were then cloned into human IgG_1 heavy constant (CH) and light constant (CL) vectors separately for expression and purification using protein A resin as described for generation of rabbit mAbs.

Hydrogen-deuterium exchange mass spectrometry

For hydrogen-deuterium exchange mass spectrometry (HDX-MS), the DDR1 stock was diluted to 5 µM (50 pmol injection) in absence (apo state) and presence of 8 µM PRTH-101 (ligand state) in non-deuterated sample buffer and kept at 1°C until labeling. For deuterium labeling, the samples were diluted 1:9 with deuterated labeling buffer (50 mM HEPES, 150 mM NaCl, pH read 7.2) and incubated for several time intervals (15 s, 1 min, 10 min, 1 hour, and 8 hour) at 20°C. Samples were quenched by mixing 1:1 with quench buffer at 1°C and immediately injected into the LC-MS system for online pepsin digestion and peptide analysis by MS using the same workflow as for peptide identification except that MS data were acquired in MS-only mode. All labeling time points were performed in triplicates.

Determination of the DDR1-DSL:PRTH-101 complex structure

The DDR1-DSL domain was generated via limited trypsin proteolysis (catalog no. T1426, Merck). PRTH-101 Fab was generated from PRTH-101 using the Pierce Fab generation kit (catalog no. 44985, Thermo Scientific) according to manufacturer's instructions. SDS-PAGE was used to identify fractions containing the DDR1-DSL:PRTH-101 complex, which were pooled for crystallization trials based on separation from the later-eluting Fc fragment. The crystal structure of DDR1-DSL:PRTH-101 complex was determined by molecular replacement using the program Phaser.[22] Models for the PRTH-101 heavy and light chains were generated from PDB ID 4AG4[23] using the program Chainsaw,[24] based on sequence alignments between the relevant chains. A model for the DSL domain of DDR1 (residues 189-367) was also generated from PDB ID 4AG4. Refinement was undertaken with initial rounds in Refmac5,[25] followed by further cycles and ultimate completion using Buster,[26] combined with manual building and real-space refinement in COOT.[27] Figures were generated using Coot[27] and Pymol.[28] The coordinates of the DDR1-DSL:PRTH-101 structure have been deposited in the Protein Data Bank (entry code 8PE9).

Collagen adhesion assay

HEK293T-WT and HEK293T-DDR1 overexpressing cells were detached using Accutase, incubated in presence of PRTH-101 or IgG isotype control for 2 hours and then seeded in plates pre-coated with human collagen I or BSA (0.5 µg/cm²) for a 60 min cell adhesion. Plates were flicked and washed with PBS twice in order to remove non-adherent cells. Adherent cells were fixed with 4% PFA for 20 min at RT and washed three times with PBS before staining with Hoechst 33342 solution (dilution 1/5000)

for 15 min at RT. All images were acquired automatically in a non-confocal mode using a HCIA Operetta system with a 5×WD objective (4 fields per well recorded) and imported for image analysis using Columbus software.

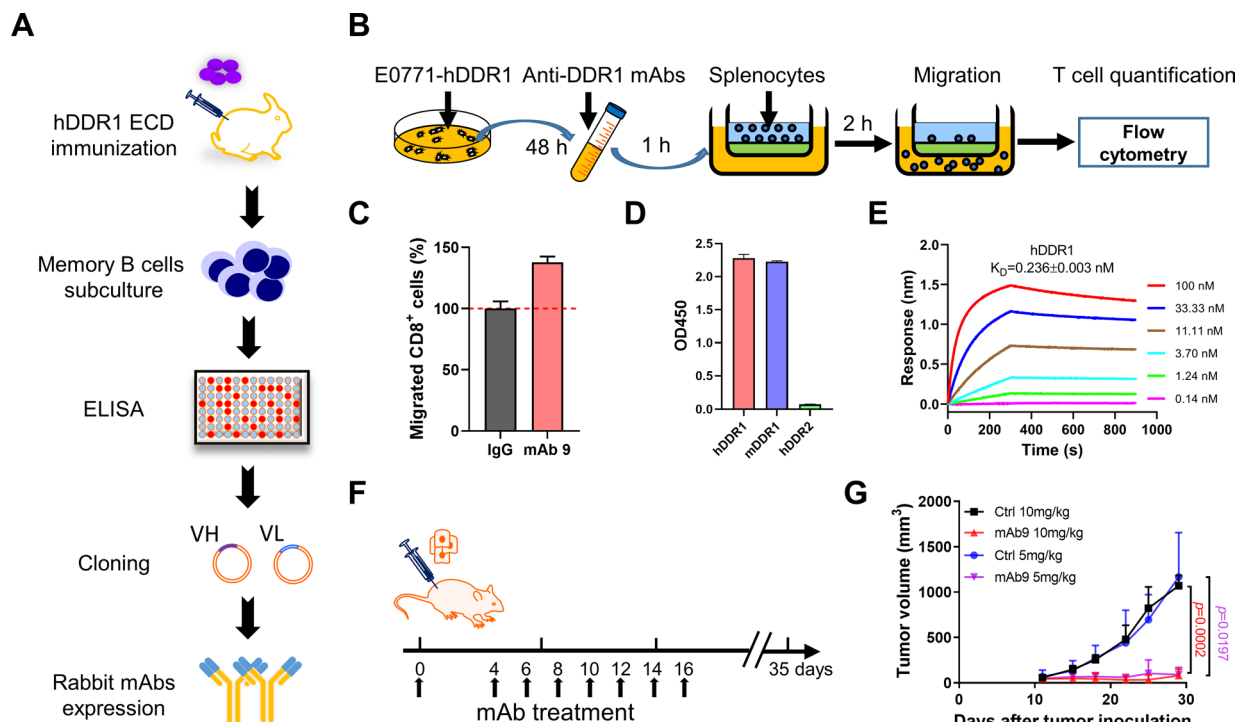## Detection of total DDR1 and phosphorylated DDR1 in cancer cell lysates

T47D cells were detached using Accutase and seeded at $1.6×10^4$ cells per well (96-well plate). After 3 days of culture (around 80% confluence), cells were serum starved overnight and stimulated with human collagen I (50 µg/mL) for 90 min. For inhibition of DDR1 phosphorylation by PRTH-101, T47D cells were preincubated with PRTH-101 or IgG control for 2 hours (dose range was 0.001–10 µg/mL with semi log scale), and collagen I was then added at a final concentration of 50 µg/mL for 90 min before making cell extracts. Cells were washed with PBS and lysed in RIPA buffer (catalog no. 89900, Thermo Scientific) supplemented with protease/phosphatase inhibitors for protein extraction. After protein quantification using BCA assay, samples were run on a JESS capillary protein detection system (Protein Simple) following the manufacturer's protocol. Detection antibody used in the assay was optimized as follows: D1G6 (for total DDR1) and E1N8F (phospho-DDR1) and Vinculin (clone hVIN-1) antibodies were 1/50, 1/50 and 1/1000, respectively.

Detection of DDR1 ECD shedding using ELISA

A sandwich ELISA was designed to quantify shed DDR1 ECD in conditional medium. LumiNunc 96-well high binding plates (catalog no. 437796, Thermo Scientific) were coated with 100 µL, 5 µg/mL of capture antibody (polyclonal rabbit anti-DDR1 mAbs purified from serum of immunized rabbits) overnight at 4°C, followed by blocking for 1 hour with 3% BSA. After washing plates with PBS buffer (pH 7.5), 100 µL of conditioned media containing shed DDR1 was added and incubated for 1 hour at RT with gentle continual shaking. After washing the plate, an in-house prepared biotinylated rabbit anti-DDR1 mAb14 (100 µL/well, 0.5 µg/mL) which does not compete with PRTH-101, was added as a secondary antibody for shed DDR1 detection, followed by strepta-vidin-HRP (dilution 1:1000, catalog no. DY998, R&D System) and Femto substrate solution (catalog no. 37075, Thermo Scientific). The relative luminescent unit at 425 nm was recorded after 3 min using a plate reader (Molecular Devices). For measuring shed DDR1 in cell culture media, cells were cultured in 96-well plates for 2 days in media with 10% FBS, then cells were washed with FBS-free media and cultured in FBS-free media containing collagen I and PRTH-101 or isotype control antibody for 24 hours before collecting the conditioned media.

Immunohistochemistry staining

Mouse mammary tumor tissues were fixed with 10% buffered formalin (catalog no. 23-427098, Fisher Scientific) at 4°C overnight. The fixed tumor samples were paraffin

Figure 1 Generation and characterization of rabbit anti-hDDR1 mAbs. (A) A cartoon showing the process to generate rabbit anti-hDDR1 mAbs. Rabbits were immunized with hDDR1 ECD (catalog no. 10730-H08H, SinoBiological) five times at 3-week intervals. Individual memory B cells were isolated 2 weeks after the last boost and the B cells were cultured for antibody expression. ELISA was used to screen the individual memory B cell cultures for hDDR1 ECD targeting antibodies. The VH and VL fragments were cloned from memory B cells that were ELISA-positive. The converted rabbit IgG$_1$ was recombinantly expressed in HEK293F cells. (B) DDR1 mAbs screened using T cell migration assay. E0771-hDDR1 was cultured for 48 hours. Conditioned media was transferred into the bottom chamber of the transwell and co-incubated with mAbs at 37°C for 1 hour. After adding splenocytes to the upper chamber, migration was performed at 37°C for 2 hours. The migratory splenocytes were collected and quantified by flow cytometry. (C) Rabbit mAb9 was assessed by quantifying migrated CD8$^+$ T cells with E0771-hDDR1 conditioned media. The results are shown as percentage normalized with isotype IgG treatment and means±SD of duplicates. (D) Binding of rabbit mAb9 (20 µg/mL) to ECDs of hDDR1, mDDR1 and hDDR2 as determined by ELISA. OD$_{450}$ values are means±SD of triplicates. (E) Binding affinity of rabbit mAb9 to hDDR1 ECD as determined by biolayer interferometry assay (BLI). (F) A cartoon showing the study design of tumor-inhibiting efficacy of the mAbs *in vivo*. C57BL/6 mice were injected with a mixture of rabbit mAbs and E0771-hDDR1 tumor cells on day 0, followed by intratumoral mAb injections on days 4, 6, 8, 10, 12, 14, and 16. Two mAb dose levels (5 and 10 mg/kg) were assessed. A rabbit IgG$_1$ isotype produced in-house was used as a control. (G) Tumor volume was measured every 4 days from day 10 after E0771-hDDR1 tumor cells inoculation. The values are shown as means±SD of duplicates. The statistical significance of the difference between 10 mg/kg of mAb treatment groups was labeled as red, purple for 5 mg/kg of mAb treatment groups. DDR1, discoidin domain-containing receptor 1; ECD, extracellular domain; mAbs, monoclonal antibodies; VH, heavy chain's variable region; VL, light chain's variable region.

embedded and sectioned into 4 µm for staining. Samples were deparaffinized in xylene, rehydrated in descending grades of ethanol and washed in PBS. Samples were boiled with antigen unmasking solution (catalog no. H-3300, Vector labs) for 20 min, blocked with 10% normal goat serum at RT for 1 hour and incubated with anti-CD3ε (dilution 1:100, catalog no. MA5-14524, Invitrogen) and anti-CD8α (dilution 1:25, catalog no. 9894, CST) at 4°C overnight. Vectastain Elite ABC-HRP kit (catalog no. PK-6105, Vector labs) with DAB substrate (catalog no. SK-4105, Vector labs) was used to detect the primary antibody. Stained samples were imaged by Nikon ECLIPSE Ti2 microscope. The percentage of CD3$^+$ and CD8$^+$ cells were quantified by QuPath software (V.0.2.3) (https://qupath.github.io). An area on the tumor side with a depth 400–600 µm from the tumor-stroma border was defined as tumor margin for CD3$^+$ and CD8$^+$ quantification.

Second harmonic generation

Mouse mammary tumor tissues were preserved at −80°C with optimal cutting temperature compound. Samples were transferred to −20°C for at least 2 hours and cut into 20 µm thick sections with a cryostat. Slides were then incubated at 37°C for 30 min and transferred to boiling antigen unmasking solution (catalog no. H-3300, Vector labs) for 10 min. Samples were nuclear stained with To-pro-3 (catalog no. T3605, Thermo Scientific) and mounted onto coverslips (No.1.5) by adding Fluoromount-G mounting media (catalog no. 100502-406, VWR). Images were acquired with a Leica TCS SP8 multiphoton confocal microscope and a 20×, HC PL Apo, NA
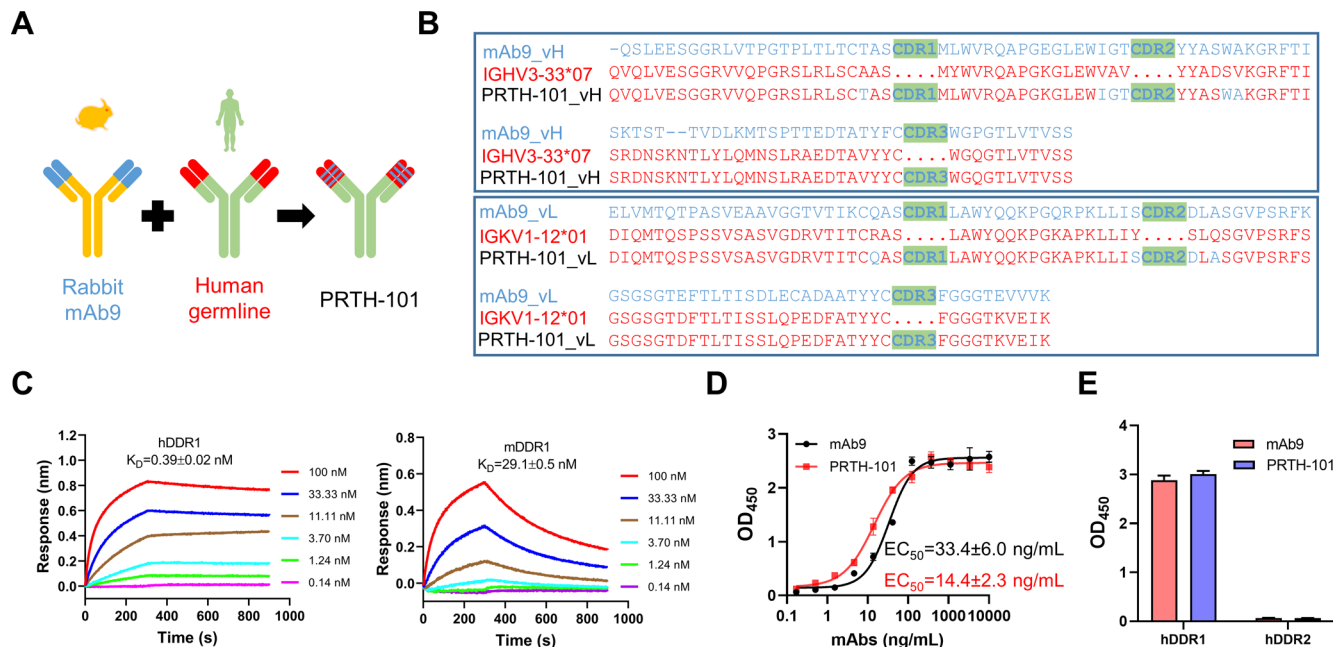
Figure 2 Humanization of rabbit mAb9 and characterization of humanized mAb PRTH-101. (A) A cartoon showing the combined KABAT/IMGT/Paratome CDR grafting strategy to humanize rabbit mAb9. (B) The heavy chain and light chain of rabbit mAb9 are shown as mAb9_vH and mAb9_vL (blue). The heavy chain and light chain of the best-matched human antibody frameworks are shown as IGHV3-33*07 and IGKV1-12*01 (red). The humanized heavy chain and light chain are shown as PRTH-101_vH and PRTH-101_vL. (C) Binding affinity of PRTH-101 to hDDR1 ECD and mDDR1 ECD as determined by BLI. (D) Binding of rabbit mAb9 and PRTH-101 to hDDR1 ECD as determined by dose-response ELISA. The antibody was serially diluted threefold from 10 µg/mL. The values are shown as means±SD of triplicates and EC_{50} was calculated by fitting a nonlinear regression (four parameter). (E) Binding of rabbit mAb9 and PRTH-101 at 10 µg/mL to the ECDs of hDDR1 and hDDR2 as determined by ELISA. OD_{450} values are means±SD of triplicates. DDR1, discoidin domain-containing receptor 1; ECD, extracellular domain.

0.7 oil-immersion objective was used throughout the experiments. Tuned excitation wavelength was 840 nm. A 420±5 nm narrow bandpass emission controlled by a slit was used to detect the second harmonic generation (SHG) signal of collagen.[29] Collagen fiber assessment was analyzed with CT Fire software (V.2.0 beta) (https://loci.wisc.edu/software/ctfire). The area on the tumor side with 400–600 µm distance from the tumor-stroma border was defined as tumor margin.

Mouse tumor model and treatment with PRTH-101

C57BL/6 mice were purchased (catalog no. 000664, Jackson Laboratory) and maintained at the animal core of George Washington University. For each *in vivo* study, 8-week-old female C57BL/6 mice were injected with E0771-hDDR1 murine tumor cells (5×10^{5} cells/mouse) into the fourth mammary fat pad. For treatment with mAb9, tumor cells and the antibody were injected as a mixture into C57BL/6 female mice (100 µL/mouse) the fourth mammary fat pad on day 0. Then mAb9 and isotype control IgG at two dose levels (5 mg/kg and 10 mg/kg) were administered intratumorally every 2 days starting on day 4 for a total of seven doses. The isotype control antibody (Rb57.4) was produced in-house using a similar production process. For the PRTH-101 antitumor efficacy study, the first antibody treatment (10 mg/kg) started on day 12 after tumors reached about 100 mm[3]

and intratumoral injections continued every other day for eight times. Tumor growth was measured using a caliper and tumor volumes were calculated using a formula (0.5×width×width×length) as reported previously.[17]

Statistical analysis

Two-tailed Student's t-test was used to compare mean differences between two groups. The observed difference between two groups was indicated by p value. All the statistics were done in GraphPad Prism V.8.0. Data are presented as mean±SD.

RESULTS

Generation and characterization of rabbit anti-hDDR1 mAbs

To select DDR1-specific mAbs, we screened a large panel of single B cell cultures (20×96 well plates) collected from DDR1 immunized rabbits. The workflow for generation and selection of mAbs is illustrated in figure 1A as reported previously.[30] Positive hDDR1 binders (122 total) identified in ELISA screening were analyzed using a functional assay for neutralizing DDR1 activity (figure 1B) before expression and purification of full length mAbs (rabbit IgG) for further characterization. A total of 31 purified rabbit anti-DDR1 mAbs were evaluated for DDR1 binding (online supplemental figure S1A) and neutralization of DDR1 function (online supplemental
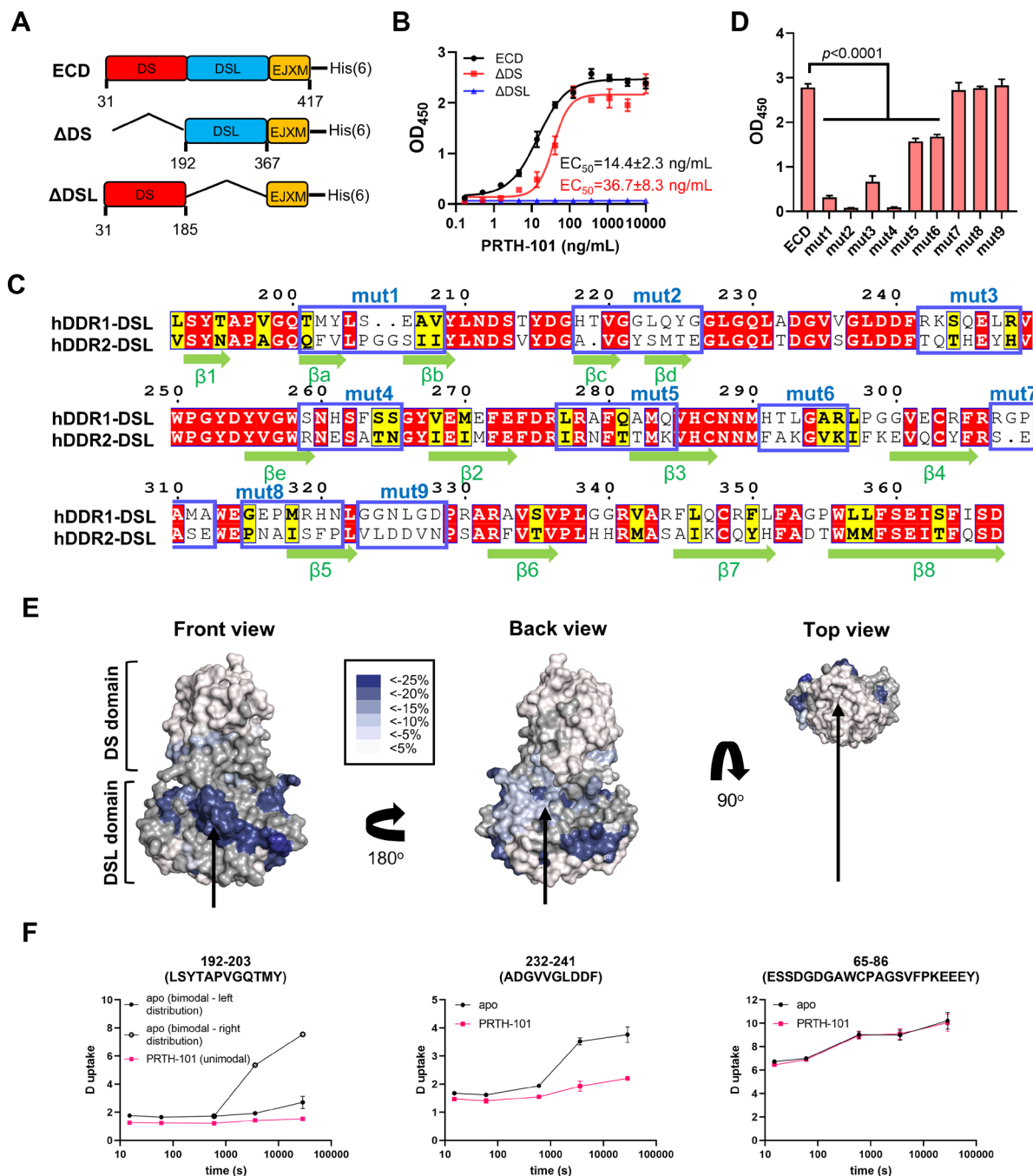
Figure 3 Epitope mapping of DDR1 interaction with PRTH-101 by mutagenesis and HDX-MS. (A) Schematic diagram showing the construction of hDDR1 ECD fragments fused to a His6-tag. DS refers to the F5/8 type C domain (residues 31–185) of hDDR1 ECD. DSL refers to the DS-like (DSL) domain (residues 192–367) of hDDR1 ECD. EJXM refers to the short extracellular juxtamembrane linker (residues 368–417). (B) Binding of PRTH-101 to hDDR1 ECD, ΔDS, and ΔDSL as determined by dose-response ELISA. PRTH-101 was threefold serially diluted from 10 μg/mL. The values are shown as means±SD of triplicates and EC50 was calculated by fitting a nonlinear regression (four parameter). (C) Alignment of hDDR1 and hDDR2 DSL domains by ESPript 3.0. As PRTH-101 binds to hDDR1, but not to hDDR2 ECD, nine hDDR1 ECD mutants were constructed by replacing hDDR1 regions with the corresponding hDDR2 sequences, and the mutation sites are boxed in blue. β strands are indicated by green arrows. (D) The binding of PRTH-101 to hDDR1 ECD and nine mutants in the DSL domain as determined by ELISA with a fixed concentration of PRTH-101 at 10 μg/mL. OD450 values are means±SD of quadruplicates. The difference between two groups was calculated by two-tailed t-test. (E) Significant H/D exchange differences after PRTH-101 binding mapped to a DDR1 crystal structure (PDB 4AG4, 1 hour labeling time point). A strong reduction in exchange in presence of PRTH-101 was seen in the DSL domain (dark blue stretch in front view, main epitope). Smaller effects were observed throughout the DSL domain, suggesting additional allosteric effects caused by PRTH-101 binding (back view). No significant changes were detected in the collagen-binding DS domain (top view). Regions with no sequence coverage are colored in gray. (F) Deuterium uptake plots of representative DDR1 peptides. Error bars reflect the standard deviation (n=3). DDR1, discoidin domain-containing receptor 1; DS, discoidin; EJXM, extracellular juxtamembrane; HDX-MS, hydrogen-deuterium exchange mass spectrometry.
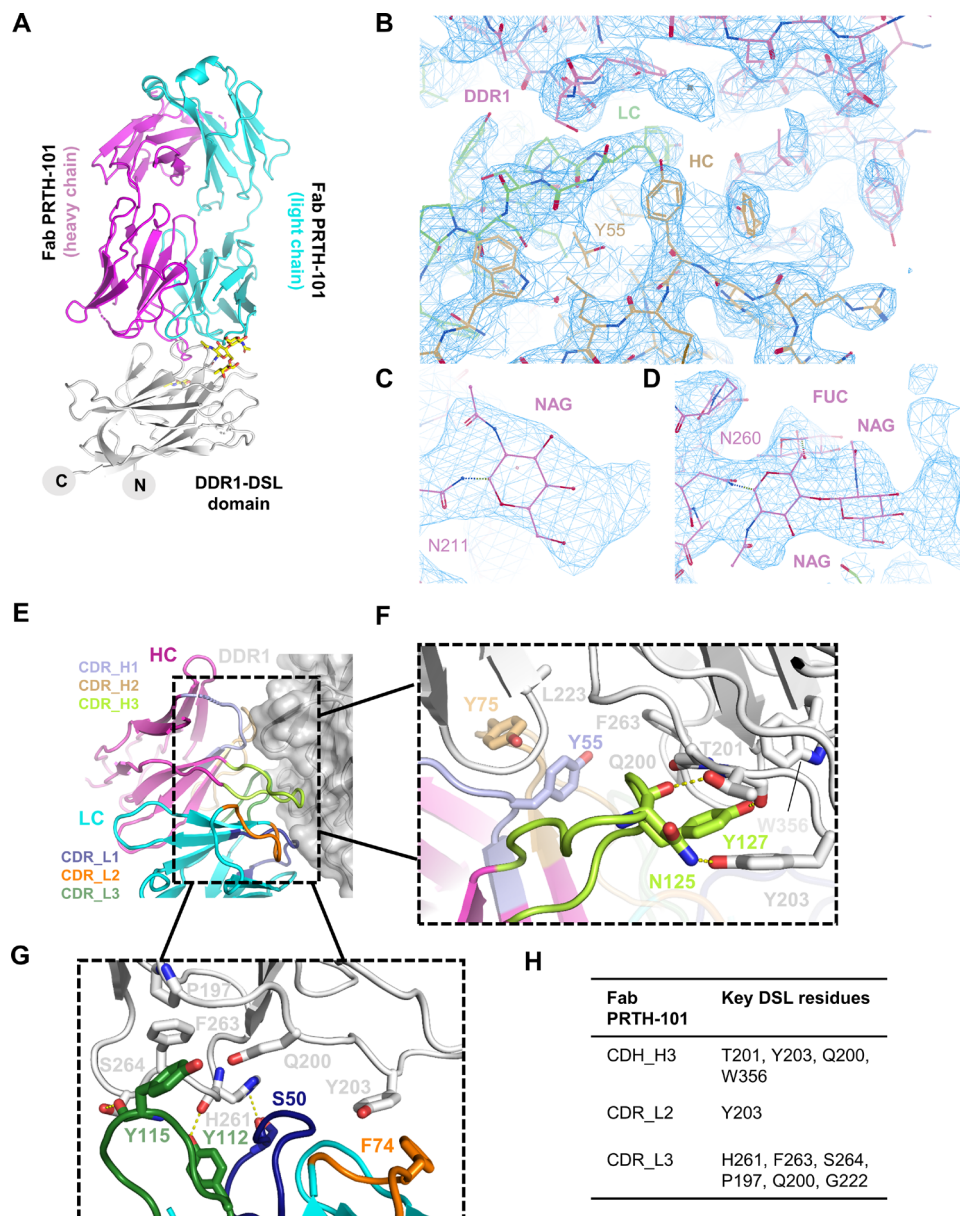
Figure 4 Epitope mapping of DDR1 interaction with PRTH-101 by X-ray crystallography. (A) Structure of DDR1-DSL in complex with PRTH-101 at 3.15 Å resolution. DDR1-DSL is shown in white, the Fab light chain in cyan, and the Fab heavy chain in magenta. N-linked sugars are displayed as sticks. (B) Close-up view of the DDR1 epitope, and interfacing CDRs from PRTH-101. (C, D) N-linked glycosylation sites on the DDR1 surface. Electron density for a single sugar at N211 (C) and a branched chain at N260 (D) are displayed. (E) The view of PRTH-101 CDRs from the heavy chain (HC, CDR_H1-3) and light chain (LC, CDR_L1-3) in complex with DDR1-DSL (transparent surface). Side chains are labeled and colored as in panel A. (F) Close-up of PRTH-101 CDRs from the heavy chain interacting with DDR1-DSL. The hydrogen bonds are displayed as dashed yellow lines. (G) Close-up of PRTH-101 CDRs from the light chain interacting with DDR1-DSL. The hydrogen bonds are displayed as dashed yellow lines. (H) The DDR1-DSL residues critical for binding of PRTH-101. DDR1, discoidin domain-containing receptor 1; DSL, discoidin-like.

figure S1B). Among the 31 purified mAbs, 15 mAbs showed both binding and neutralizing activity, and mAb9 was selected as a lead mAb for further characterization (figure 1C). The mAb9 showed cross binding to both human and mouse DDR1 (mDDR1), but no binding to human DDR2 (hDDR2) (figure 1D). The binding affinity (K_D) of mAb9 to hDDR1 is in the subnanomolar range (0.236 nM, figure 1E), and the binding affinity of mAb9 to mDDR1 is at 15.4 nM (online supplemental figure

S1C). Consistent with previously published results,[17] antitumor efficacy of mAb9 *in vivo* using a syngeneic mouse tumor model with E0771-hDDR1 cells in C57BL/6 mice abolished tumor growth at both 5 and 10 mg/kg dosing levels (figure 1F,G).

Humanization of rabbit mAb9
Since mAb9 was isolated from an immunized rabbit, we conducted humanization of the antibody to enable
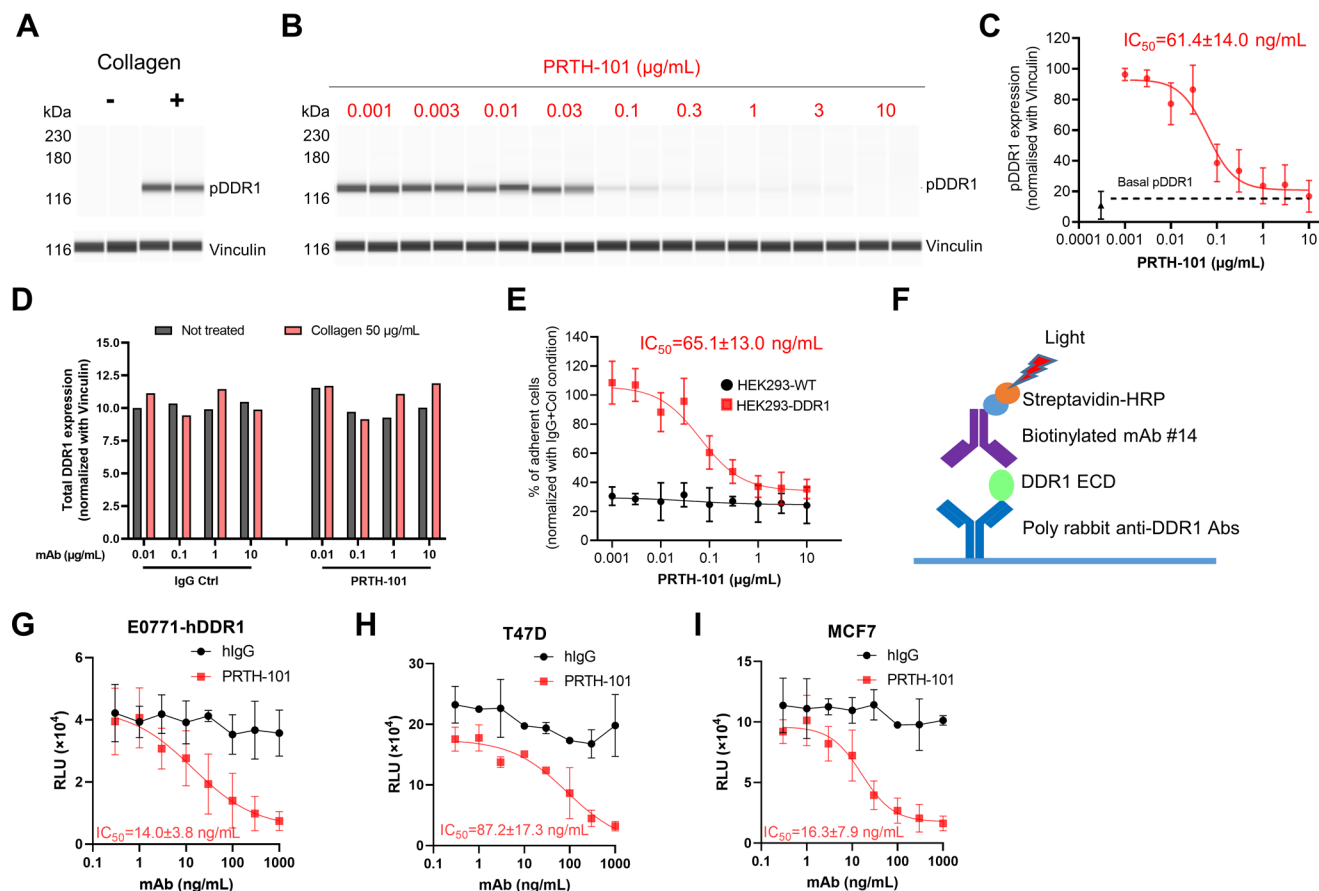
Figure 5 Functional characterization of PRTH-101 using DDR1 phosphorylation, collagen adhesion, and DDR1 shedding assays. (A) Induction of pDDR1 in T47D cells with collagen (50 µg/mL) treatment. Vinculin and pDDR1 were detected in cell lysates by JESS technology. Individual capillaries run in the same experiment are shown. (B) Digital representation of data obtained for pDDR1 and Vinculin detection with different concentrations of PRTH-101 treatment. T47D cells were pre-incubated for 2 hours in presence of PRTH-101 or IgG control at different concentrations. Then collagen I was added at a final concentration of 50 µg/mL and pDDR1 was measured by JESS after 90 min of stimulation. Samples from the same experiment were run in individual capillaries. (C) Representation of IC_{50} determination using data from at least two individual experiments (two replicates per condition). The IC_{50} value was determined as best fit of data by nonlinear regression analysis. (D) Total DDR1 expression was measured by JESS with same method described in panel B. (E) PRTH-101 inhibited adhesion of HEK293 cells overexpressing hDDR1 to collagen I-coated plates. IC_{50} was determined by nonlinear regression analysis of cell adhesion assay data from at least three individual experiments (four replicates per condition). (F) A cartoon showing the process of sandwich ELISA to detect shed DDR1. The generation of shed DDR1 from E0771-hDDR1 (G), T47D (H) and MCF-7 (I) cell cultures was inhibited by PRTH-101 in a dose-dependent manner. The IC_{50} values were calculated as best-fit values of shed DDR1 data from three replicates. DDR1, discoidin domain-containing receptor 1.

advancement of the antibody into preclinical and clinical development. We grafted CDRs sequences from the rabbit IgG (mAb9, in blue) into best-matched IgG human germline framework sequences to generate PRTH-101 (figure 2A). As shown in figure 2B, the best-matched human germlines (in red) for mAb9 were IGHV3-33*07 and IGKV1-12*01 for heavy chain (in top box) and light chain (in bottom box), respectively. The CDRs (highlight in green boxes) of mAb9 were inserted into the human germline framework sequences of heavy chain and light chains to generate humanized antibody PRTH-101. Binding affinities of PRTH-101 for hDDR1 and mDDR1 are similar to its parental mAb9 with K_D values of 0.39 nM and 29.1 nM, respectively (figure 2C). The EC_{50} for PRTH-101 binding to hDDR1 ECD of 14.4±2.3 ng/mL as measured by ELISA is also comparable to the

EC_{50} of 33.4±6.0 ng/mL measured for parental mAb9 (figure 2D). Similarly, humanized PRTH-101 maintains specificity for hDDR1 ECD and does not bind to hDDR2 (figure 2E).

Binding epitope of PRTH-101

The ECD of hDDR1 is composed of DS domain, DSL domain, and extracellular juxtamembrane region.[31] To identify the binding epitope of PRTH-101, we made domain fragments of hDDR1 ECD lacking either the DS domain (ΔDS) or the DSL domain (ΔDSL) with a C-terminal His_6 for purification (figure 3A). Binding of PRTH-101 to the ΔDSL fragment was completely abolished, while the binding to ΔDS protein was maintained with an EC_{50} of 36.7±8.3 ng/mL in comparison with that for hDDR1 ECD (14.4±2.3 ng/mL) (figure 3B). Follow-on
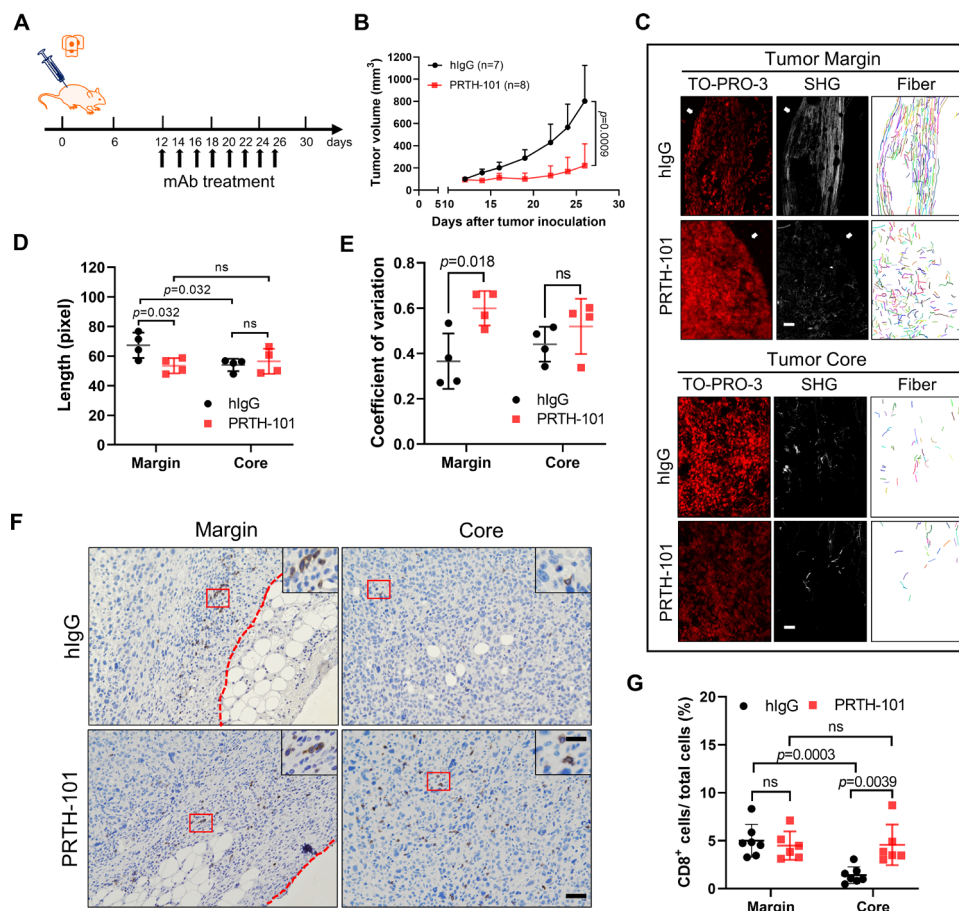
Figure 6 The antitumor activity of PRTH-101 in C57BL/6 mice. (A) A cartoon showing the process of testing the antitumor activity of PRTH-101 *in vivo*. Mice were injected with E0771-hDDR1 cells in the mammary fat pad. Antibodies were intratumorally injected on day 12 every other day when the tumors reached about 100 mm³. (B) The tumor growth curve after mice were treated with IgG control and PRTH-101. The values were shown as means±SD. The difference between two groups was calculated by two-tailed Student's t-test. n (hIgG)=7, n (PRTH-101) = 8. (C) Representative images of tumor margin and core analyzed by TO-PRO-3 staining (red), SHG (gray), and collagen fiber individualization (far right panel). Scale bar: 50 μm. (D) Quantification of collagen fiber length in tumor margin and core. The values were shown as means±SD. The difference between two groups was compared by two-tailed t-test. n (hIgG)=4, n (PRTH-101) = 4. (E) Coefficient of variation of collagen fiber in tumor margin and core are quantified. The difference between two groups was calculated with two-tailed t-test. n (hIgG)=4, n (PRTH-101) = 4. (F) Representative IHC images of CD8^{+} T cells in tumor margin and core of antibody-treated tumors. Scale bar: 50 μm, scale bar (inlet): 20 μm. An area on the tumor side with a depth of 400–600 μm from the tumor-stroma border was defined as tumor margin, which is indicated by the red dashed line. (G) Quantification of CD8^{+} T cells in tumor margin and core for antibody-treated tumors. The difference between two groups was calculated by two-tailed t-test. n (hIgG)=7, n (PRTH-101)=6. IHC, immunohistochemistry; ns, not significant; SHG, second harmonic generation.

mutagenesis experiments to identify the PRTH-101 epitope focused on the DSL domain. Since PRTH-101 did not bind hDDR2, we generated hDDR1/hDDR2 chimeras (boxed region, figure 3C) by replacing non-conserved hDDR1 peptide sequences with corresponding hDDR2 peptide sequences (online supplemental table S1). We made nine DDR1 chimeric mutants (mut1-9) for evaluation of binding by PRTH-101 in comparison with wild-type hDDR1 ECD using ELISA (figure 3D). Among the nine chimera constructs, hDDR1 mut1 (AA 201-208), mut2 (AA 218–226) and mut4 (AA 259-265) largely abolished binding of PRTH-101, whereas mut3 (AA 242-248), mut5 (AA 277-284) and mut6 (AA 291-296) showed significant reduction of PRTH-101 binding, suggesting that those mutated regions are critical for PRTH-101

binding (figure 3D). In contrast, mut7, mut8, and mut9 maintained binding of PRTH-101, suggesting the regions in mut7 (AA 307-312), mut8 (AA 315-321), and mut9 (AA 323-328) are not critically involved in PRTH-101 binding to hDDR1 ECD (figure 3D).

We next performed HDX-MS to further identify the binding sites of PRTH-101 on hDDR1 ECD. Detailed experimental and statistical analyses are summarized in online supplemental table S2. DDR1 peptide identification with optimized quenching buffer conditions resulted in 75% sequence coverage (online supplemental figure S2A). The results showed that PRTH-101 binding resulted in a significant protection from H/D exchange in large parts of the DSL domain as mapped onto the DDR1 structure (figure 3E, front view, online

supplemental figure S2B). Strong reduction in deuterium uptake is especially detectable at longer labeling times, and effects on deuterium (D) uptake for the peptides (AA 192–203, LSYTAPVGQTMY) are shown in figure 3F and online supplemental figure S3. Weaker protection is seen in peptides covering the lower part of the collagen binding DS domain and the back of the DSL domain (AA 232–241, ADGVVGLDDF, figure 3E, back view, figure 3F). This could be due to spatial or allosteric effects by PRTH-101 binding to the DSL domain. There were no significant differences detected at the collagen binding site located in the DS domain[23 32] (AA 65–86, ESSDGDGA WCPAGSVFPKEEEY, figure 3E, top view, figure 3F). The critical peptides identified by HDX-MS analysis are consistent with the findings in the chimeric mutation assay.

To further identify key amino acid residues in DDR1 ECD that contribute to the PRTH-101 binding epitope, we solved a crystal structure of DDR1-DSL complexed to PRTH-101 to 3.15Å resolution (figure 4A, online supplemental table S3). Initial trials using the full-length DDR1 ECD did not produce crystallization hits, and therefore a truncated DDR1 construct was generated via limited proteolysis using trypsin. A single copy of a DDR1-DSL:PRTH-101 complex was observed in the asymmetric unit of the resulting crystals, with both variable regions of the Fab well resolved (figure 4B), as well as 2 N-linked glycans on residues N211 and N260 of DDR1 (figure 4C,D). All 6 CDRs from PRTH-101 interact with the DDR1-DSL domain, covering 1589Å^2 (~1/8th) of the solvent-accessible surface of DDR1-DSL, and CDR3 from both heavy and light chains are positioned in the center of the interface (figure 4E). Residues N125 and Y127 from CDR_H3 play a key role in the interaction with DDR1, contributing hydrogen bonds with DDR1 residues T201 and Y203 (figure 4F). Additionally, CDR_H3 residue Y127 has the greatest buried surface area of any heavy chain residue in the interface (99Å^2) and contributes van der Waals contacts through interactions with DDR1 residues Q200, Y203 and W356 (figure 4F), as does CDR_L2 residue F74 through contacts with DDR1 residue Y203 (figure 4G). Key tyrosine side chains from CDR3_L3 are also involved in the interaction, with Y112 forming a hydrogen bond with the main chain of DDR1 H261, and Y115 forming a pi-stacking interaction with DDR1 F263, a main-chain hydrogen bond with S264 and van der Waals contacts with P197, Q200 and G222 (figure 4G). Importantly, the key amino acid residues (figure 4H) contributing to the PRTH-101 binding epitope identified by the X-ray crystal structure are consistent with the protected peptides identified by HDX-MS analysis (online supplemental figure S4). In conclusion, PRTH-101 binds the DSL domain of DDR1, distal from the collagen binding site on the DS domain.

PRTH-101 inhibits DDR1 phosphorylation and shedding from cancer cells

To understand the mechanisms of action of PRTH-101, we assayed the inhibitory activity of PRTH-101 on collagen-mediated DDR1 functions. As it is well documented that collagen triggers phosphorylation of DDR1,[18] we determined whether antibody PRTH-101 can inhibit DDR1 phosphorylation using a human breast cancer cell line (T47D). Treatment of T47D cells with human collagen I induced strong DDR1 phosphorylation in presence of an isotype control antibody (figure 5A), and addition of PRTH-101 resulted in dose-dependent inhibition of pDDR1 with an IC$_{50}$ value of 61.4±14.0 ng/mL (figure 5B,C). Interestingly, treatment with PRTH-101 did not alter total DDR1 levels in cancer cells in presence or absence of collagen (figure 5D, online supplemental figure S5). We also assayed the effects of PRTH-101 on collagen-mediated cell adhesion. Pre-incubation of DDR1-expressing cells (HEK293-DDR1) with PRTH-101 blocked cell adhesion to collagen with an IC$_{50}$ of 65.1±13.0 ng/mL (figure 5E, online supplemental figure S6). As collagen induces DDR1 shedding from cells,[20] we investigated effects of PRTH-101 treatment on DDR1 shedding using DDR1-expressing E0771-hDDR1 transfectants and the two human breast cancer cell lines T47D and MCF7 (online supplemental figure S7). We measured shedding of DDR1 in cancer cell media using a sandwich ELISA (figure 5F). First, we determined that shedding of DDR1 in cancer cell cultures reached a plateau at a collagen concentration of 50 µg/mL (online supplemental figure S8). Then we tested effects of antibody PRTH-101 on DDR1 shedding in the presence of collagen at 50 µg/mL. Treatment with PRTH-101 effectively blocked DDR1 shedding with an IC$_{50}$ of 14.0±3.8 ng/mL for E0771-hDDR1 cells, 87.2±17.3 ng/mL for T47D cells, and 16.3±7.9 ng/mL for MCF7 cells (figure 5G–I). We assessed levels of full length DDR1 and the cleaved DDR1 (without ECD due to shedding) in cell lysates of T47D and MCF7 cells by Western blotting. Cancer cells were treated with PRTH-101 mAb in the presence of collagen (50 µg/mL) and isotype antibody (hIgG) as the treatment control (online supplemental figure S9). T47D cancer cells had higher levels of full length DDR1 than that of MCF7 cells. There was no clear difference in the presence or absence of PRTH-101 mAb treatment in comparison with the isotype IgG control, but there was a visible decrease of the cleaved DDR1 in PRTH-101 mAb treated cells (online supplemental figure S9, left image). Interestingly, we detected visibly higher levels of full length DDR1 and lower levels of the cleaved DDR1 in the MCF7 cells in the PRTH-101 mAb treated cell lysates in comparison with that in the isotype hIgG control cell lysates (online supplemental figure S9, right image). The differences between the two cancer cell lines may be due to the differences in DDR1 expression levels. The results showed that PRTH-101 treatment inhibited the shedding of DDR1, which is consistent with our data of shed DDR1 in the medium as measured by ELISA.

PRTH-101 disrupts collagen alignment and enhances T cell tumor infiltration *in vivo*

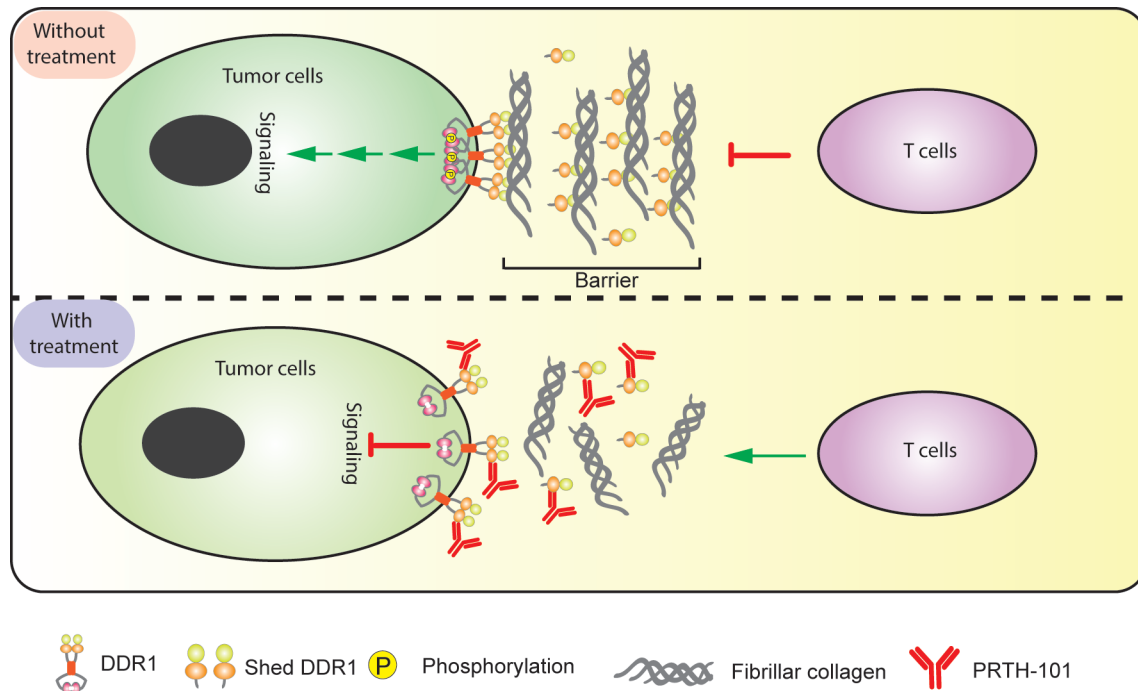We examined the antitumor effect of PRTH-101 using the murine syngeneic tumor model E0771-hDDR1 in

Figure 7 A model showing multiple mechanisms of PRTH-101 contributing to antitumor activity. Top: Collagen fiber binds to DDR1 homodimer on the cell surface and induces its oligomerization. Simultaneously, downstream DDR1 signaling and shedding of DDR1 ECD are activated. The shed DDR1 facilitates collagen fiber alignment and immune exclusion. Bottom: PRTH-101 prevents oligomerization of DDR1 homodimer to block downstream signaling and DDR1 ECD shedding. The low level of shed DDR1 is captured by PRTH-101 and the collagen fiber alignment is disrupted which results in immune cell infiltration. DDR1, discoidin domain-containing receptor 1; ECD, extracellular domain.

C57BL/6 mice with every other day injections of PRTH-101 at 10 mg/kg (figure 6A). Compared with the IgG isotype control group, PRTH-101 showed robust anti-tumor efficacy (figure 6B). To investigate how PRTH-101 impacts collagen alignment in the extracellular matrix (ECM) and immune cell infiltration in tumors, we examined collagen fiber alignment using SHG imaging and immunohistochemistry (IHC) staining of T cells in tumor margins and cores. PRTH-101 treated tumors had significantly shorter collagen fibers in the tumor margin than mice treated with hIgG isotype control (figure 6C, top panel, figure 6D), while there was no difference in collagen fiber length in tumor cores from mice treated with PRTH-101 and isotype control (hIgG) (figure 6C, bottom panel, figure 6D). Similarly, the coefficient of variation of the angle at the tumor margin was also significantly increased in tumor margins from mice treated with PRTH-101 in comparison with that from the isotype control group, while there was no difference detected in tumor cores from PRTH-101-treated and isotype control treated groups (figure 6E). Collagen fiber width and straightness are comparable between the PRTH-101 and isotype hIgG control groups in either the tumor margin or tumor core (online supplemental figure S10A,B). Analysis of CD8+ and total T cell infiltration (CD3+) using IHC showed that treatment with PRTH-101 significantly increased both total T cells (online supplemental figure S11) and CD8+ T cell infiltration into the tumor core, while there were no differences in the tumor margins

in comparison with isotype hIgG (figure 6F,G). When comparing T cell infiltration between tumor margin and tumor core, the isotype hIgG control group had significantly lower T cell density in the tumor core than in the tumor margin due to IE (figure 6G), while PRTH-101 treated tumors had similar CD8+ (figure 6G) and total T cell densities (online supplemental figure S11). These *ex vivo* analyses indicate that PRTH-101 disrupted collagen alignment in the tumor margin and thereby overcame T cell exclusion from the tumor core.

DISCUSSION
DDR1 plays an important role in signal transduction and regulates multiple physiological and pathological processes, such as cell proliferation, differentiation, migration, apoptosis and matrix remodeling.[33] More and more evidence suggested that dysregulation of DDR1 contributes to human disease development, especially cancer.[9 34] In recent years, a number of researchers have attempted to target DDR1 signaling therapeutically to treat cancer with a focus on inhibition of DDR1 tyrosine kinase activity.[10 35–37] Several DDR1 inhibitors targeting the tyrosine kinase have been reported, such as imatinib, nilotinib and 7rh.[38] However, these efforts have been hampered by specificity issues of these inhibitors and relatively modest single agent antitumor activity in preclinical cancer models.[36] Recently, our group reported a new finding on the role of DDR1 ECD in orchestrating tumor

IE by organizing tumor collagen into dense fibrils.[17] This study reports that humanized monoclonal antibody PRTH-101 specifically targets DDR1 ECD and blocks both intracellular DDR1 phosphorylation and extracellular interactions between collagens and DDR1, making PRTH-101 a promising therapeutic development candidate, which has entered clinical trials in April 2023 for patients with advanced malignancies (ClinicalTrials.gov Identifier: NCT05753722).

The PRTH-101 binding epitope on the DSL domain is distinct from the structure reported for antibody 3E3.[23] Unlike 3E3, which binds DDR1 ECD near its C terminus, PRTH-101 binds to DDR1 on the βα-βe region between β1 and β2, which is 'opposite' to the 3E3 binding region (online supplemental figure S12), resulting in important functional differences. For example, antibody 3E3 inhibited DDR1 activity without blocking collagen binding, whereas PRTH-101 also inhibited DDR1-mediated cell adhesion to collagen.

Understanding the mechanism of antibody action is critical for development of cancer therapeutics. In this study, we revealed that PRTH-101 suppressed DDR1 activity by multiple mechanisms outlined in figure 7, which include inhibition of DDR1 phosphorylation and shedding of DDR1 from cells. *Ex vivo* analyses of tumor tissues revealed disruption of collagen fiber alignment in the tumor ECM and enhanced T cell infiltration into tumor cores. Based on the binding epitope for PRTH-101, it is plausible that PRTH-101 does not directly compete with collagen binding to DDR1, since the epitope of PRTH-101 is located on the DDR1 DSL domain, while collagen binds to the neighboring DS domain. We tested whether PRTH-101 impacted the binding between DDR1 ECD (His tagged) and collagen using an Octet-based binding assay. The collagen binding after PRTH-101 binding to DDR1 was reduced in comparison with the isotype control hIgG (online supplemental figure S13). We do not consider PRTH-101 as a competitive inhibitor of collagen binding of DDR1 as we would expect zero collagen binding in presence of 200 nM PRTH-101, which is $>100 \times K_D$. The data are consistent with an allosteric mechanism of inhibition, the nature of which we do not yet fully understand. Also consistent with allostery is the fact that the inhibitory effect of PRTH-101 appears to saturate between 50 and 200 nM. Binding of PRTH-101 to the DSL domain may reduce the affinity of DDR1 for collagen. Several studies have reported that oligomerization of DDR1 increased interaction of DDR1 with collagen in comparison to monomeric interaction with collagen in solution.[18 39 40] Furthermore, DDR1 oligomers exhibit stronger binding to collagen compared with dimeric DDR1.[41] Another study has shown that DDR1 exists as a stable homodimer on the cell surface, independent from collagen binding and activation.[42] Conversely, stimulation by collagen leads to oligomerization of DDR1, and formation of oligomers triggers intracellular DDR1 autophosphorylation and further downstream signaling.[43] PRTH-101 may inhibit oligomerization of DDR1 on the cell surface, and therefore, reduce collagen interactions with DDR1. Future investigation is warranted to determine whether and how PRTH-101 blocks oligomerization of DDR1.

Full-length DDR1 is a tyrosine kinase receptor expressed on cell membranes and extracellular domains. It can be cleaved from cell surface-expressed DDR1 as soluble DDR1 and interacts with collagen in ECM.[20] On the other hand, collagen fibers deposited in the cell microenvironment play a crucial role in ECM remodeling. The deposited ECM is considered as the primary physical impediment to T cell infiltration.[6] A TNBC tumor that has an immune excluded microenvironment with an absence of CD8^{+} T cells is associated with fibrotic stroma and poor clinical outcome.[3] Therefore, DDR1 may play a critical role in the IE phenotype of TNBC and likely other tumor types. Zhong *et al* found that DDR1 expression levels in breast cancer tissues are higher than that in adjacent normal tissue, and that DDR1 regulated tumor growth by modulating tumor-infiltrating T cells.[11] While we only focused on the impact on T cell functions by an anti-DDR1 therapy in the current study, we can not exclude the possibility of an impact on other immune cell subsets. It will be interesting to examine the impact of anti-DDR1 therapies on additional immune subsets beyond T cells.

A study has reported that collagen binding to DDR1 induced shedding of DDR1 by ADAM10 at the AA407 and AA408 site.[20 44] Based on our analysis of binding epitope of PRTH-101, amino acid residues 407 and 408 are part of a low complexity stretch of residues (370–415), rich in Pro, Gly, Ser, and Asn residues. This makeup typically causes regions to be unstructured, facilitating access of a protease to a cleavage site in this region. The resolved C-terminal boundary of the DSL domain in our crystal structure is N370, and there are 37 (predicted) disordered residues between the C-terminus of the DSL domain and the proteolytic cleavage site. Therefore, we hypothesize that inhibition of DDR1 shedding by PRTH-101 may function through interfering in the binding of DDR1 to collagen and blocking collagen-mediated oligomerization of DDR1, since shedding of DDR1 depends on collagen interaction with DDR1. Further, the reduced DDR1 shedding by PRTH-101 may result in the disruption of collagen fiber formation in the tumor ECM. Collectively, our results demonstrated that the DDR1-targeting PRTH-101 resulted in reduced shedding of DDR1 ECD, which may contribute to the disruption of collagen fiber formation in ECM and enhanced T cell infiltration.

Author affiliations
[1]Texas Therapeutics Institute, Brown Foundation Institute of Molecular Medicine, The University of Texas Health Science Center at Houston, Houston, Texas, USA
[2]Department of Biochemistry and Molecular Medicine, The George Washington University, Washington, DC, USA
[3]Evotec (France) SAS, Campus Curie, 195 route d'Espagne, 31036 Toulouse CEDEX, Toulouse, France
[4]Evotec (UK) Ltd, Abingdon, UK
[5]Evotec SE, Manfred Eigen Campus, Hamburg, Germany

[6]Department of Biochemistry and Molecular Biology, University of Texas Medical Branch, Galveston, Texas, USA
[7]Parthenon Therapeutics Inc, Boston, Massachusetts, USA

ORCID iDs
Samuel C Griffiths http://orcid.org/0000-0002-9257-7354
Jasmin Dülfer http://orcid.org/0000-0001-9614-7645
Zhiqiang An http://orcid.org/0000-0001-9309-2335
Thomas Schürpf http://orcid.org/0000-0003-3023-1136

REFERENCES

1 Binnewies M, Roberts EW, Kersten K, *et al*. Understanding the tumor immune Microenvironment (TIME) for effective therapy. *Nat Med* 2018;24:541–50.
2 Kalinski P, Talmadge JE. Tumor immune Enviroment in cancer progression and cancer therapy. *Adv Exp Med Biol* 2017;1036:1–18.
3 Gruosso T, Gigoux M, Manem VSK, *et al*. Spatially distinct tumor immune Microenvironments stratify triple-negative breast cancers. *J Clin Invest* 2019;129:1785–800.
4 Fu T, Dai L-J, Wu S-Y, *et al*. Spatial architecture of the immune Microenvironment Orchestrates tumor immunity and therapeutic response. *J Hematol Oncol* 2021;14.
5 Kather JN, Suarez-Carmona M, Charoentong P, *et al*. Topography of cancer-associated immune cells in human solid tumors. *Elife* 2018;7:e36967.

6 Pai SI, Cesano A, Marincola FM. The paradox of cancer immune exclusion: immune oncology next frontier. *Cancer Treat Res* 2020;180:173–95.
7 Carafoli F, Hohenester E. Collagen recognition and Transmembrane signalling by Discoidin domain receptors. *Biochim Biophys Acta* 2013;1834:2187–94.
8 Majo S, Auguste P. The Yin and Yang of Discoidin domain receptors (Ddrs): implications in tumor growth and metastasis development. *Cancers (Basel)* 2021;13:1725.
9 Gao Y, Zhou J, Li J. Discoidin domain receptors Orchestrate cancer progression: A focus on cancer therapies. *Cancer Sci* 2021;112:962–9.
10 Valiathan RR, Marco M, Leitinger B, *et al*. Discoidin domain receptor tyrosine Kinases: new players in cancer progression. *Cancer Metastasis Rev* 2012;31:295–321.
11 Zhong X, Zhang W, Sun T. Ddr1 promotes breast tumor growth by suppressing antitumor immunity. *Oncol Rep* 2019;42:2844–54.
12 Mehta V, Chander H, Munshi A. Complex roles of Discoidin domain receptor tyrosine Kinases in cancer. *Clin Transl Oncol* 2021;23:1497–510.
13 Yang SH, Baek HA, Lee HJ, *et al*. Discoidin domain receptor 1 is associated with poor prognosis of non-small cell lung Carcinomas. *Oncol Rep* 2010;24:311–9.
14 Park H, Kim K, Lee H, *et al*. Overexpression of Discoidin domain receptor 1 increases the migration and invasion of hepatocellular carcinoma cells in association with matrix metalloproteinase. *Oncol Rep* 2007;1435–41.
15 Shimada K, Nakamura M, Ishida E, *et al*. Prostate cancer Antigen-1 contributes to cell survival and invasion though Discoidin receptor 1 in human prostate cancer. *Cancer Sci* 2008;99:39–45.
16 Reger de Moura C, Battistella M, Sohail A, *et al*. Discoidin domain receptors: A promising target in Melanoma. *Pigment Cell Melanoma Res* 2019;32:697–707.
17 Sun X, Wu B, Chiang H-C, *et al*. Tumour Ddr1 promotes collagen fibre alignment to instigate immune exclusion. *Nature* 2021;599:673–8.
18 Leitinger B. Molecular analysis of collagen binding by the human Discoidin domain receptors, Ddr1 and Ddr2. identification of collagen binding sites in Ddr2. *J Biol Chem* 2003;278:16761–9.
19 Leitinger B. Discoidin domain receptor functions in physiological and pathological conditions. *Int Rev Cell Mol Biol* 2014;310:39–87.
20 Vogel WF. Ligand-induced shedding of discoidin domain receptor 1. *FEBS Lett* 2002;514:175–80.
21 Zhang YF, Ho M. Humanization of rabbit Monoclonal antibodies via Grafting combined Kabat/IMGT/Paratome Complementarity-determining regions: rationale and examples. *MAbs* 2017;9:419–29.
22 McCoy AJ, Grosse-Kunstleve RW, Adams PD, *et al*. Phaser Crystallographic software. *J Appl Crystallogr* 2007;40:658–74.
23 Carafoli F, Mayer MC, Shiraishi K, *et al*. Structure of the Discoidin domain receptor 1 extracellular region bound to an inhibitory Fab fragment reveals features important for signaling. *Structure* 2012;20:688–97.
24 Stein N. CHAINSAW: a program for Mutating Pdb files used as Templates in molecular replacement. *J Appl Crystallogr* 2008;41:641–3.
25 Murshudov GN, Vagin AA, Dodson EJ. Refinement of macromolecular structures by the maximum-likelihood method. *Acta Crystallogr D Biol Crystallogr* 1997;53:240–55.
26 Bricogne G. *ea. BUSTER version 2.11.8*. Cambridge, United Kingdom: Global Phasing Ltd, 2021.
27 Emsley P, Lohkamp B, Scott WG, *et al*. Features and development of Coot. *Acta Crystallogr D Biol Crystallogr* 2010;66:486–501.
28 System TPMG. *Version 20 Schrodinger LLC*.
29 Erikson A, Örtegren J, Hompland T, *et al*. Quantification of the second-order Nonlinear susceptibility of collagen I using a laser scanning microscope. *J Biomed Opt* 2007;12:044002.
30 Gui X, Deng M, Song H, *et al*. Disrupting Lilrb4/APOE interaction by an efficacious Humanized antibody reverses T-cell suppression and blocks AML development. *Cancer Immunol Res* 2019;7:1244–57.
31 Agarwal G, Smith AW, Jones B. Discoidin domain receptors: Micro insights into macro assemblies. *Biochim Biophys Acta Mol Cell Res* 2019;1866:S0167-4889(19)30102-8.
32 Carafoli F, Bihan D, Stathopoulos S, *et al*. Crystallographic insight into collagen recognition by Discoidin domain receptor 2. *Structure* 2009;17:1573–81.
33 Yeh YC, Lin HH, Tang MJ. Dichotomy of the function of Ddr1 in cells and disease progression. *Biochim Biophys Acta Mol Cell Res* 2019;1866:S0167-4889(19)30074-6.
34 Borza CM, Pozzi A. Discoidin domain receptors in disease. *Matrix Biol* 2014;34:185–92.

35 Rammal H, Saby C, Magnien K, *et al*. Corrigendum: Discoidin domain receptors: potential actors and targets in cancer. *Front Pharmacol* 2016;7:346.

36 Elkamhawy A, Lu Q, Nada H, *et al*. The journey of Ddr1 and Ddr2 kinase inhibitors as rising stars in the fight against cancer. *Int J Mol Sci* 2021;22:6535.

37 Kothiwale S, Borza CM, Lowe EW, *et al*. Discoidin domain receptor 1 (Ddr1) kinase as target for structure-based drug discovery. *Drug Discov Today* 2015;20:255–61.

38 Guo J, Zhang Z, Ding K. A patent review of Discoidin domain receptor 1 (Ddr1) Modulators (2014-present). *Expert Opin Ther Pat* 2020;30:341–50.

39 Mihai C, Iscru DF, Druhan LJ, *et al*. Discoidin domain receptor 2 inhibits Fibrillogenesis of collagen type 1. *J Mol Biol* 2006;361:864–76.

40 Agarwal G, Mihai C, Iscru DF. Interaction of Discoidin domain receptor 1 with collagen type 1. *J Mol Biol* 2007;367:443–55.

41 Yeung D, Chmielewski D, Mihai C, *et al*. Oligomerization of Ddr1 ECD affects receptor-ligand binding. *J Struct Biol* 2013;183:495–500.

42 Noordeen NA, Carafoli F, Hohenester E, *et al*. A Transmembrane Leucine Zipper is required for activation of the dimeric receptor tyrosine kinase Ddr1. *J Biol Chem* 2006;281:22744–51.

43 Corcoran DS, Juskaite V, Xu Y, *et al*. Ddr1 Autophosphorylation is a result of aggregation into dense clusters. *Sci Rep* 2019;9:17104.

44 Shitomi Y, Thøgersen IB, Ito N, *et al*. Adam10 controls collagen signaling and cell migration on collagen by shedding the Ectodomain of Discoidin domain receptor 1 (Ddr1). *Mol Biol Cell* 2015;26:659–73.
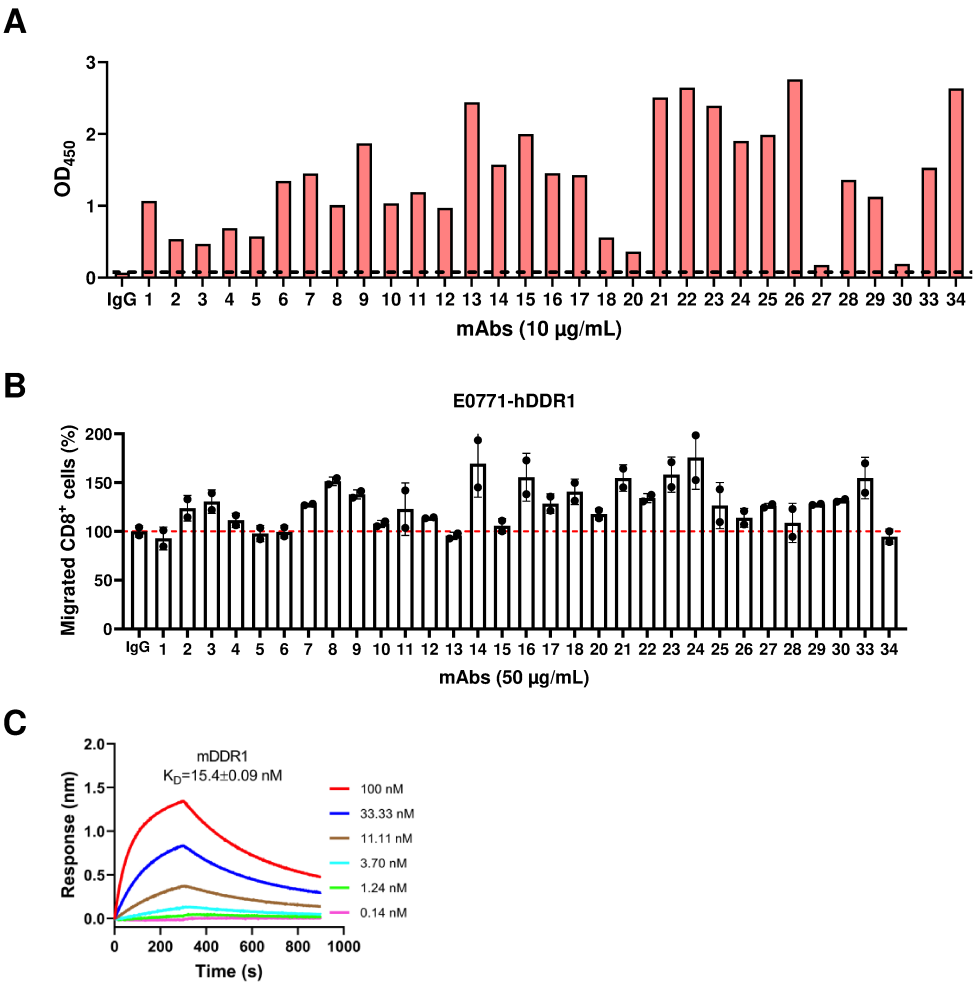
Supplemental material

BMJ Publishing Group Limited (BMJ) disclaims all liability and responsibility arising from any reliance placed on this supplemental material which has been supplied by the author(s)

J Immunother Cancer

Figure S1 Screening of anti-hDDR1 ECD rabbit mAbs. (A) Binding of the 31 recombinantly expressed and purified rabbit mAbs to hDDR1 ECD as determined by ELISA. The dashed line is the OD_{450} of a control rabbit IgG1 as a cut-off for binders. (B) The 31 mAbs were assessed for their activity to enhance CD8+ T cells migration mediated by E0771-hDDR1 conditioned media. The migrated CD8+ cells were normalized with a rabbit isotype IgG1 produced in-house. The red dashed line indicates the migrated CD8+ cells treated by rabbit isotype IgG1. (C) Binding affinity of rabbit mAb9 to mDDR1 ECD as determined by Octet RED96.

Table S1 Nine DDR1-DSL mutants which contain amino acids switch from hDDR1 to hDDR2.

Mutants	hDDR1	hDDR2	AA
mut1	TMYLSEAV	QFVLPGGSII	201-208
mut2	HTVGGLQYG	AVGYSMTE	218-226
mut3	RKSQELR	TQTHEYH	242-248
mut4	SNHSFSS	RNESATN	259-265
mut5	LRAFQAMQ	IRNFTTMK	277-284
mut6	HELGAR	FAKGVK	291-296
mut7	RGPAMA	SEASE	307-312
mut8	GEPMRHN	PNAISFP	315-321
mut9	GGNLGD	VLDDVN	323-328

Table S2 Summary of HDX-MS analysis for the PRTH-101-DDR1 epitope mapping experiment.

Data Set	apo (control)	PRTH-101
HDX reaction details	non-deuterated sample buffer (50 mM HEPES, 150 mM NaCl, pH 7.2); deuterated labeling buffer (50 mM HEPES, 150 mM NaCl, pHread 7.2); quench buffer (1 M glycine, 4 M GndHCl, 200 mM TCEP, pH 2.5); labeling temperature 20°C; HDX labeling dilution 1:9; protein amount 50 pmol	
HDX time course (sec)	15, 60, 600, 3600, 28800	15, 60, 600, 3600, 28800
HDX control samples	none	none
Back-exchange (mean / IQR over entire project)	unknown	unknown
# of peptides	98	98
Sequence coverage	75.42%	75.42%
Average peptide length / Redundancy	11.64 / 2.75	11.64 / 2.75
Replicates	3	3
Repeatability (avg. stddev of #D)	0.1375	0.1363
Significant differences in HDX (delta HDX > X D)	0.5771 D	

Supplemental material

BMJ Publishing Group Limited (BMJ) disclaims all liability and responsibility arising from any reliance placed on this supplemental material which has been supplied by the author(s)

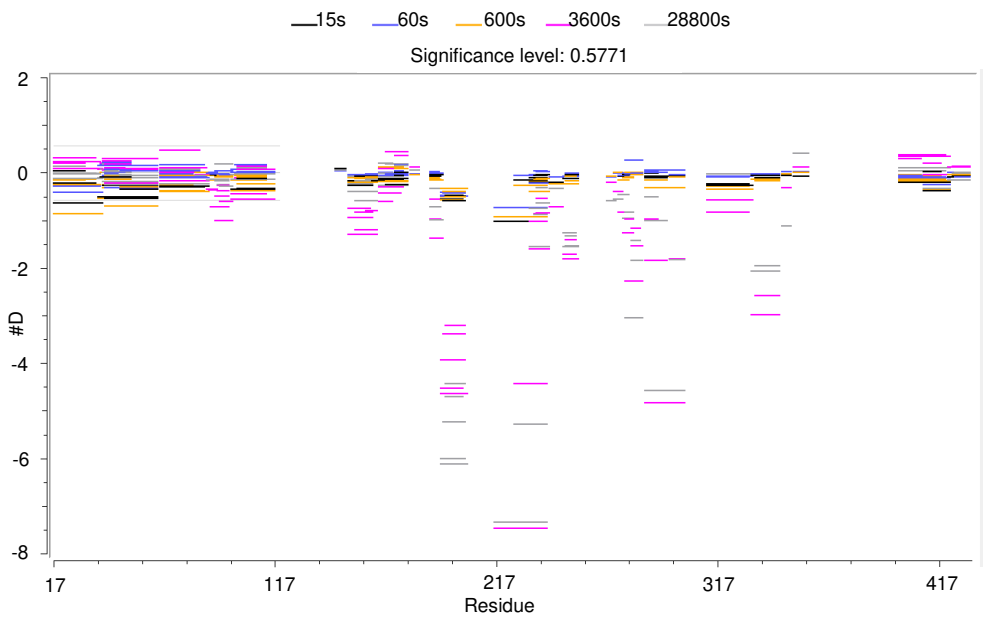*J Immunother Cancer*

A

B

Figure S2 HDX-MS to identify the binding sites of PRTH-101. (A) DDR1 effective peptide coverage map for HDX-MS experiments with PRTH-101. Sequence coverage was 75.4 %. (B) Woods plot for PRTH-101-DDR1 epitope mapping. Depicted are deuteration differences from centroid analysis at different labeling time points in individual comparison experiments (PRTH-101–apo). In case of bimodal spectra the higher deuterated peak distribution was used for HDX difference calculation. The significance level was calculated as 0.5771 Da.
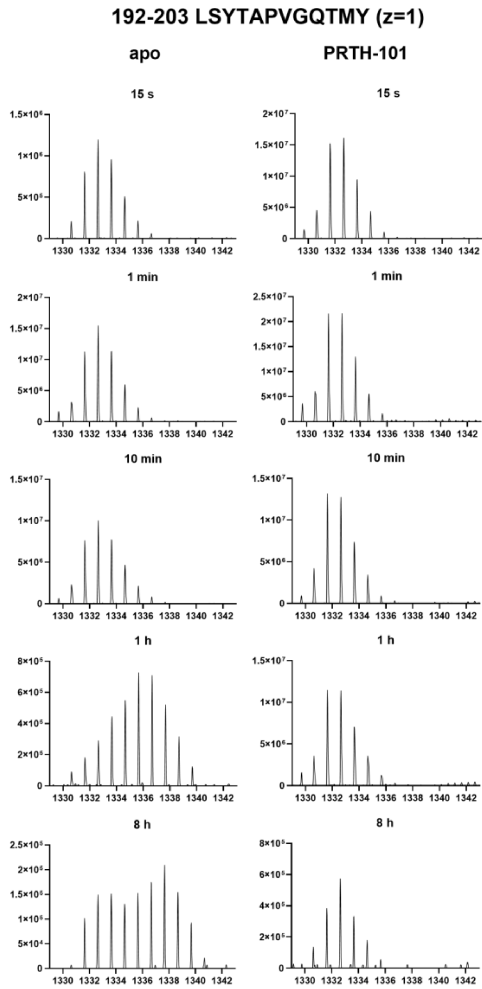
Figure S3 Spectra comparison of DDR1 peptide 192-203 in the apo state and with PRTH-101 bound. In the apo state bimodal peak distributions are visible at 1 h and 8 h labeling time points. These could be the result of mixed exchange kinetics caused by slow local dynamics of the protein which are absent in the PRTH-101 bound state.

Table S3 Data collection and refinement of the DDR1-DSL:PRTH-101 complex. Values in parenthesis correspond to the highest resolution shell.

|	
Data collection	
Space group	$P2_12_12$
Cell dimensions	
a, b, c (Å)	117.1, 144.5, 52.3
α, β, γ (°)	90, 90, 90
Ellipsoidal resolution cut-offs, a, b, c (Å)	3.6, 3.1, 4.0
Wavelength (Å)	1.00001
Synchrotron, beamline	Swiss Light Source, PXI
Resolution (Å)	72.3 - 3.15 (3.56-3.15)
No. of unique observations	9760 (488)
Completeness (%)	86 (47)
Multiplicity	6.0 (6.7)
$\langle I/\sigma(I) \rangle$	7.0 (1.8)
R_{merge} (%)	27.1 (99.3)
R_{pim} (%)	17.7 (59.2)
$CC_{1/2}$	0.99 (0.61)
Refinement	
Resolution	72.22 - 3.15
Number of reflections (test set)	9760 (496)
R_{work}/R_{free} (%)	27.8 / 30.9
No. of atoms:	
Protein	4588
Sugar	52
Metal ions	5
Average B-factor (Å^2):	
Protein	68.9
Sugar	78.7
Metal ions	82.2
RMSD bond lengths (Å)	0.007
RMSD bond angles (°)	1.23
Ramachandran plot (%)	
Favoured	93.3
Allowed	6.5
Outliers	0.2

RMSD = Root Mean Square Derivative
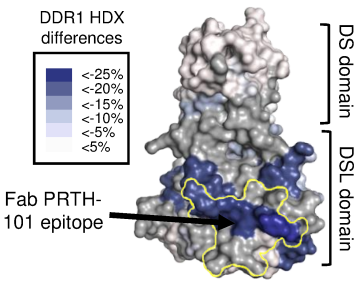
Figure S4 Comparison between protected peptides identified by HDX-MS and epitope from X-ray crystal structure. Overlap of the PRTH-101 epitope on the DDR1-DS and DSL domain surface with HDX data (based on PDB ID 4AG4). The epitope identified by the crystal structure is shown using a yellow outline. Observed deuteration differences are mapped onto the DDR1-DSL domain surface using a blue-to-red scale, as displayed by the inset.
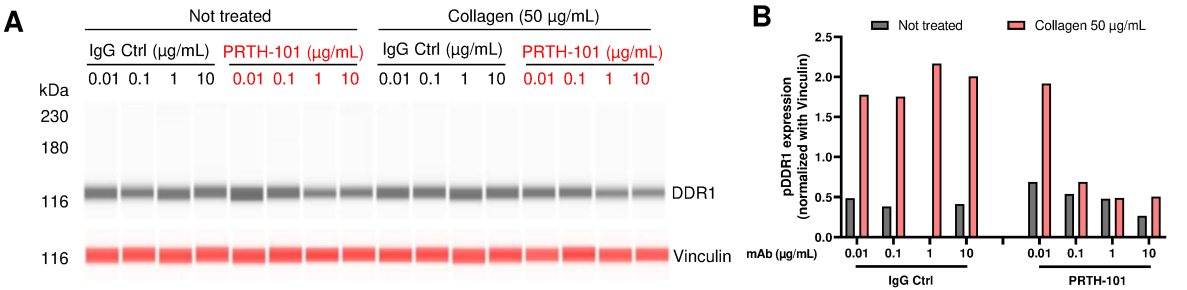

Figure S5 PRTH-101 inhibits DDR1 phosphorylation, but not alter total DDR1 expression. (A) Digital representation of data obtained for total DDR1 and Vinculin detection with different concentrations of IgG and PRTH-101 treatment. (B) pDDR1 was measured by JESS with different concentrations of IgG and PRTH-101 treatment.
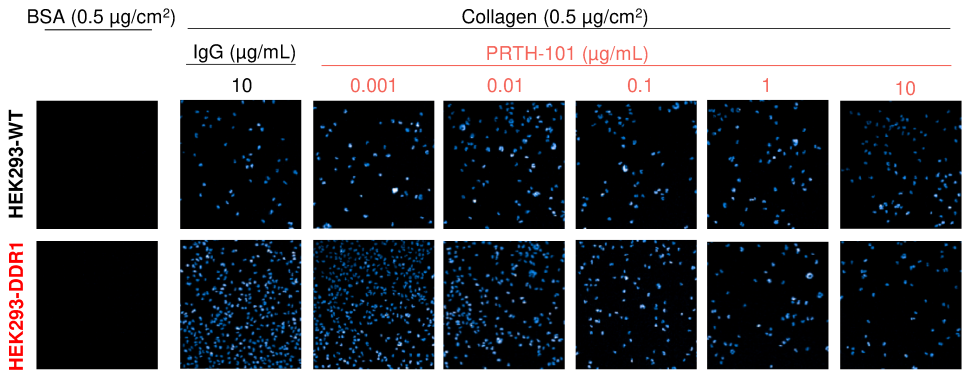

Figure S6 Functional characterization of PRTH-101 using collagen adhesion. Pictures of cell adhesion after 60 min using nuclei staining (Hoechst 33342). HEK293-WT or HEK293-DDR1 cells were detached and incubated for 2 h with/without IgG control or PRTH-101 for 2 h. Cells were seeded in plates coated with collagen I or BSA ($0.5\ \mu g/cm^2$).

Supplemental material

BMJ Publishing Group Limited (BMJ) disclaims all liability and responsibility arising from any reliance placed on this supplemental material which has been supplied by the author(s)
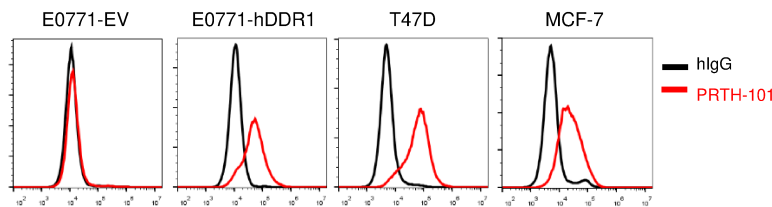
J Immunother Cancer

Figure S7 The binding of hIgG control and PRTH-101 to engineered E0771-EV, E0771-hDDR1, T47D and MCF-7 were determined with flow cytometry. Alexa Fluor 633 labelled goat anti-human IgG (H+L) was used as secondary antibody.
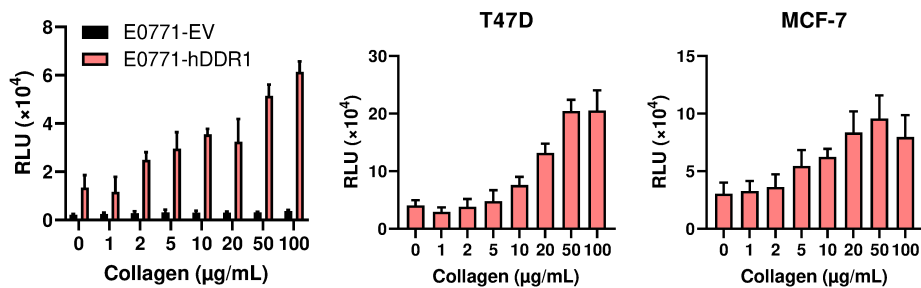

Figure S8 E0771-EV, E0771-hDDR1, T47D and MCF-7 were treated with different doses of collagen and shed DDR1 in the supernatant was detected by sandwich ELISA.
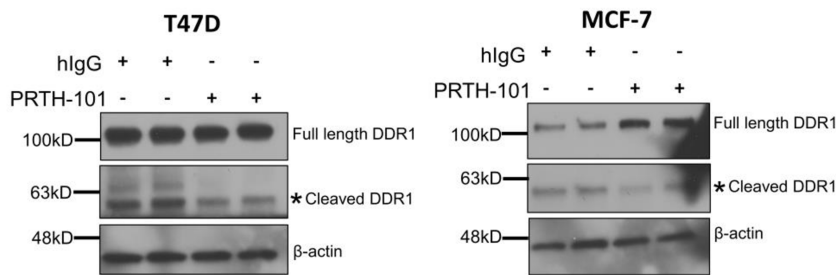

Figure S9 Assessment of full-length and cleaved DDR1 following PRTH-101 treatment in T47D and MCF-7 cell lysates using western blot detection. Cleaved DDR1 is for DDR1 after shedding DDR1 ECD. Antibody treated cells (24 hours) were washed with PBS twice and RIPA buffer was used to lysate cells. Cell lysates were used for WB detection. Full length and cleaved DDR1 on cell surface were detected by western blot using antibody D1G6 (Cell Signaling, #5583). Each treatment was duplicated.
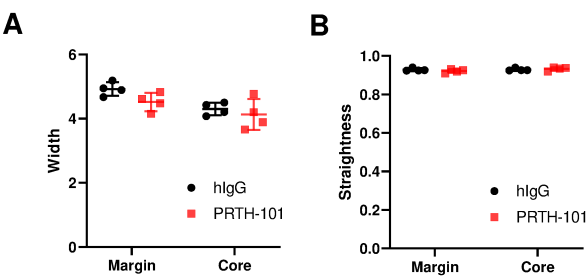
Supplemental material

BMJ Publishing Group Limited (BMJ) disclaims all liability and responsibility arising from any reliance placed on this supplemental material which has been supplied by the author(s)

J Immunother Cancer

Figure S10 Comparison of collagen width (A) and straightness (B) in tumor margin and tumor core within hIgG or PRTH-101-treated tumors. The difference between two groups was calculated with two-tailed t-test.
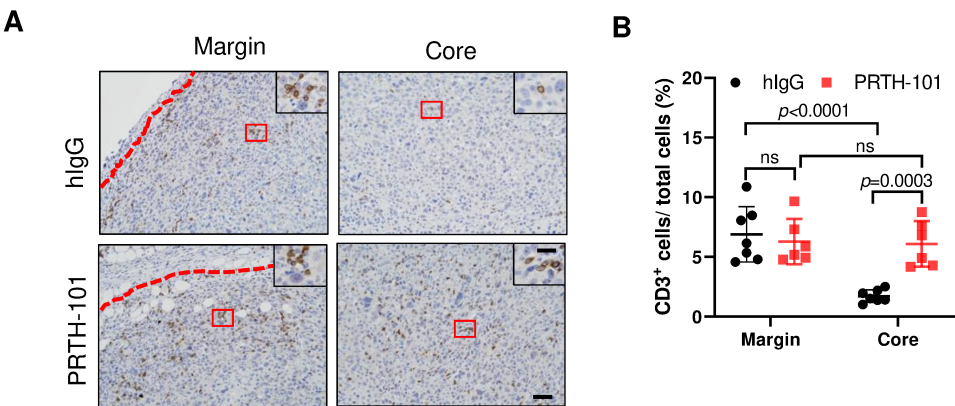

Figure S11 (A) Representative IHC images of CD3$^+$ T cells in tumor margin and core for antibody-treated tumor. Scale bar: 50 µm, scale bar (inlet): 20 µm. An area on the tumor side with a depth 400-600 µm from the tumor-stroma border was defined as tumor margin which was separated by red dash line. (B) Quantification of CD3$^+$ T cells in tumor margin and core for antibody-treated tumor. The difference between two groups was calculated with two-tailed t-test. n (hIgG) = 7, n (PRTH-101) = 6.
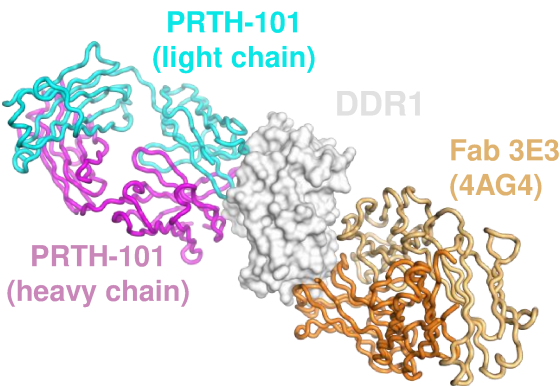

Figure S12 Comparison of the DDR1-DSL:PRTH-101 structure with published anti-DDR1 Fab 3E3 (PDB ID 4AG4, colored orange). Structures were superposed based on the DDR1-DSL domain. PRTH-101 and DDR1-DSL are colored as in figure 4A.
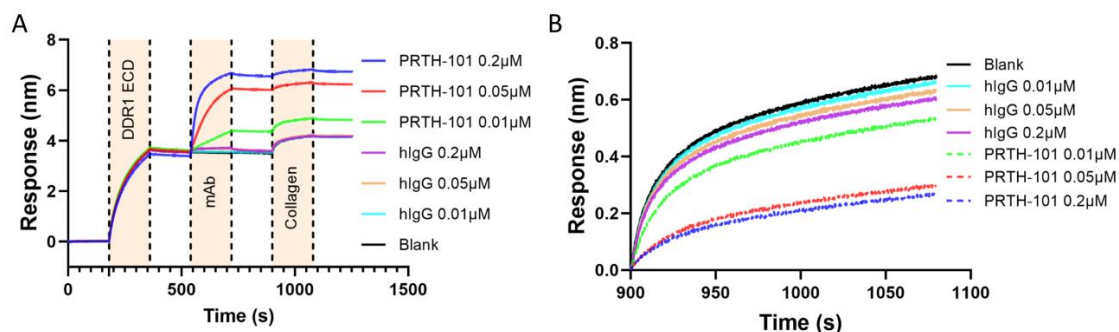
Figure S13 An *in vitro* Octet analysis of DDR1 ECD binding to collagen in the presence and absence of PRTH-101. (A) The binding response in Octet96Red system to test whether PRTH-101 impact the binding of DDR1 ECD to collagen. DDR1 ECD with His tag was captured by NTA-Ni sensor. After incubating with 30 µg/mL of isotype hIgG or PRTH-101, the sensor was dipped into 0.2 µM of collagen to test the binding response. Between each step the sensor was balanced in kinetic buffer for 180 s. (B) The response of collagen binding step after normalized with baseline control at 900 s. PRTH-101 treatments were marked as dash lines.